LANGMUIR

pubs.acs.org/Langmuir Article

3D Printing of Cellulose Nanocrystal-Loaded Hydrogels through Rapid Fixation by Photopolymerization

Doron Kam, Ariel Braner, Avi Abouzglo, Liraz Larush, Annalisa Chiappone, Oded Shoseyov,* and Shlomo Magdassi*

Cite This: https://doi.org/10.1021/acs.langmuir.1c00553 Read Online

ACCESS | Metrics & More | Article Recommendations | Supporting Information

ABSTRACT: New ink compositions for direct ink writing (DIW) printing of hydrogels, combining superior rheological properties of cellulose nanocrystals (CNCs) and a water-compatible photoinitiator, are presented. Rapid fixation was achieved by photopolymerization induced immediately after the printing of each layer by 365 nm light for 5 s, which overcame the common height limitation in DIW printing of hydrogels, and enabled the fabrication of objects with a high aspect ratio. CNCs imparted a unique rheological behavior, which was expressed by orders of magnitude difference in viscosity between low and high shear rates and in rapid high shear recovery, without compromising ink printability. Compared to the literature, the presented printing compositions enable the use of low photoinitiator concentrations at a very short build time, 6.25 s/mm, and are also curable by 405 nm light, which is favorable for maintaining viability in bioinks.

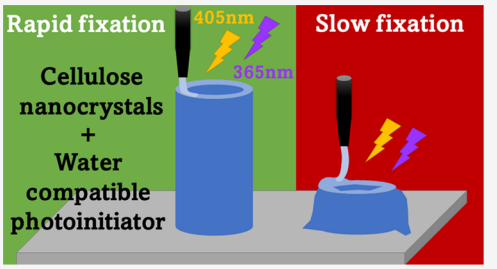

INTRODUCTION

Three-dimensional (3D) printing, also known as additive manufacturing, has become an important fabrication technology during the past decade and has already been implemented in a variety of fields, such as automotives,[1] aerospace,[2] dentistry,[3] soft robotics,[4] and even pharmaceutics.[5] In particular, 3D bioprinting, which addresses current challenges in medicine, such as bone scaffold and even printed heart mimics composed of hydrogels, is an emerging and continuously evolving field.[6−8] The most common 3D bioprinting technology for printing hydrogel is based on extrusion, also known as direct ink writing (DIW), which forms objects by extruding successive layers of materials, layer after layer, along a predesigned pathway. Other hydrogel-based printing techniques, such as vat photopolymerization[9] and material jetting systems,[10] yield high resolution far beyond that needed for biological purposes. In addition, currently, the cell composition of the tissue/organ and the bioinks is a major obstacle when using these techniques due to clogging of nozzles by cells or the lack of vat multimaterial printing technology. Therefore, despite the limited resolution of extrusion-based printing as compared to vat polymerization and material jetting, it is plausible that it will remain the preferred technology for bioprinting clinically relevant constructs.[11]

3D printing through extrusion-based technologies requires (1) sufficient ink viscosity to maintain it in the extruder, (2) ink flow, achieved by applying pressure during the extrusion, (3) shape fidelity, achieved by retaining high viscosity upon contact with the printer platform, and (4) rapid fixation to prevent the collapse of the printed structure.

Shape fidelity in DIW is very challenging, due to conflicting ink specifications, which are governed by ink rheology properties that tackle gravity and surface energy. When the printed material does not undergo a rapid fixation process, the printed object can slump after exceeding a certain height due to gravity, a height that is determined by the rheological ink properties. For example, for 45 wt % Boehmite suspension, slumping already occurs at a height of 5 mm.[12] To obtain greater heights, the ink yield stress must be increased; however, this interferes with the printability of the ink. Alternatively, tall objects can be fabricated by inducing an immediate increase in viscosity of the printed structure during the printing process via a photopolymerization reaction, as performed in inkjet printing by the Polyjet technology.[13] Inkjet printing requires inks with very low viscosities, which are not suitable for printing high-viscosity polymer solutions.

DIW combined with UV photopolymerization has been used to print hydrogels composed of gelatin methacryloyl.[14,15] The printing compositions contained the photoinitiator (PI) Irgacure 2959, which is water-soluble but has very low absorption in the wavelengths that are relevant to current

Received: February 25, 2021
Revised: May 6, 2021

3D printers (365−405 nm).[16] Thus, to achieve rapid and efficient photopolymerization, there is a need for a water-soluble PI that absorbs well at the relevant wavelengths. Therefore, here, we utilize our recently reported water-compatible PI 2,4,6-trimethylbenzoyl-diphenylphosphine oxide (TPO), which by itself is not soluble in water.[17] TPO is suitable for photopolymerization at 405 nm, which is favorable for bioprinting and cell viability. Rapid fixation to obtain high-aspect-ratio objects cannot be achieved by photopolymerization alone due to time-lapse between the point of extrusion and the point at which the ink meets light irradiation. Therefore, we used a dual-fixation mechanism, based on both polymerization and rheology. The latter can be achieved using cellulose nanocrystals (CNCs), which is a biocompatible material that has been shown to be favorable for DIW.[18,19]

CNCs are nanometric rod particles, which originate from cellulose hydrolysis mainly by sulfuric acid.[20,21] CNC integration in photopolymerizable hydrogels was mainly achieved by its chemical or physical entrapment within a hydrated polymer network.[22] Chemical modification of CNC by polymerizable groups, such as acrylates and methacrylates, may impair its water dispersibility and, therefore, the water medium should be replaced by solvents.[23,24] Poly(*N*,*N*-dimethacrylamide) (PDMA) hydrogels were reinforced by acrylated CNCs dispersed in water in the presence of 2,2′-diethoxyacetophenone (Irgacure 2959), the most common water-soluble PI at that time. However, the polymerization reaction required 50 min, which is too long a time for rapid fixation in DIW processes.[25]

A previous study on the physical entrapment of CNCs demonstrated hydrogel fabrication in molds with inks containing CNC with various monomers. 2,2-Diethoxyacetophenone was used as a photoinitiator in a photopolymerization process that was carried out for 1 h.[26] Later, the same group used different PIs and UV-polymerized the ink for 3 h.[27] Zhang et al. used dimethyl sulfoxide (DMSO) as the liquid medium for DIW and Irgacure 2959 and applied UV irradiation for 10 min.[28] Frost et al. used lithium phenyl-2,4,6-trimethylbenzoylphosphinate (LAP) as a water-soluble PI for DIW printing and reported polymerization within 60 s in a UV postcuring chamber.[29] There are also some reports on the application of inks containing CNC in vat printing processes, where photopolymerization is faster than in DIW but occurs within a thinner layer of ink, in the micron-size range.[30−32]

Figure S1 summarizes the literature data regarding photopolymerization-based fabrication of 3D hydrogel objects including CNC, emphasizing the long duration required to achieve photopolymerization of hydrogels and the high concentration of PI that is needed; due to the high water content in typical hydrogels, their reactivity is usually low, thus requiring light exposure times that are too long for practical purposes.

Here, we present new hydrogel compositions for DIW printing, which utilizes the unique pseudoplastic behavior of CNC, combined with rapid fixation of the printed objects by photopolymerization. The developed formulations composed of CNC and water-compatible PIs enable the unprecedented reduction of exposure times, down to approximately 5 s, which results in the most rapid buildup rate (Figure S1). Using the proposed ink compositions, hydrogels with high aspect ratios, excellent shape fidelity, and superior mechanical properties can be achieved in a rapid printing process.

MATERIALS AND METHODS

Materials. Cellulose nanocrystal (CNC) freeze-dry powder was obtained from Celluforce Inc., Montreal, Canada (freeze-dry, LOT #2015-009). Acrylic acid (AA), isopropanol (IPA), and poly(ethylene glycol) hexadecyl ether (Brij 58) were purchased from Sigma-Aldrich. Poly(ethylene glycol) diacrylate (PEGDA) was obtained as a gift from Sartomer-Arkema (SR610, France). PI 2,4,6-Trimethylbenzoyl-diphenylphosphine oxide (TPO) was kindly given by IGM Resins (Omnirad TPO, the Netherlands).

Water-Compatible PI. A water-compatible powder composed of 5 wt % 2,4,6-trimethylbenzoyl-diphenylphosphine oxide (TPO) PI and 95 wt % Brij 58 was prepared based on previous publications.[17,33] Upon addition of 1 wt % to water or the hydrogel ink composition, it forms a clear solution.

Ink Preparation. A 10 wt % dispersion of CNC in TDW was prepared by sonication (Vibra-Cell, Sonics & Materials) (750W, 15 min, pulses of 2 s on, 1 s pause) in an ice water bath to prevent overheating. The obtained dispersion was mixed with the other materials, as indicated in Table 1, using a planetary mixer for 5 min and was defoamed for 2 min (AR-100, THINKY Co., Ltd., Japan). The final ink compositions were kept in a 10 mL disposable syringe without exposure to light.

Table 1. Ink Compositions

	0% CNC	1.2% CNC	2.4% CNC	3.6% CNC	5.8% CNC
10%CNC [g]	0	5	10	15	23.2
AA [g]	17.3	16.85	16.4	15.95	15.2
TDW [g]	23.2	18.2	13.2	8.2	0
PEGDA [g]	0.9	0.88	0.86	0.83	0.8
TPO-Brij [g]	0.9	0.88	0.86	0.83	0.8

Rheology. Rheology measurements were performed at room temperature (20 °C) using a Haake Rheostress 6000 rheometer (Thermo Fisher Scientific, Waltham, MA) coupled with an RS6000 temperature controller (lower plate, TMP 350; upper plate, P35TiL; gap, 0.5 mm). All experiments started at a constant low shear rate ($\dot{\gamma}$ = 0.01 1/s, t = 100 s, T = 20 °C) to reach the set temperature and achieve a defined shear history before the actual experiment. Then, for the viscosity−shear rate curves, the shear rate was ramped up from $\dot{\gamma}$ = 0.01 1/s to $\dot{\gamma}$ = 100 1/s at t = 100 s. For thixotropic measurements, the shear rate was ramped up from $\dot{\gamma}$ = 0.01 1/s to $\dot{\gamma}$ = 100 1/s, then held at a maximum shear rate (MSR; $\dot{\gamma}$ = 100 1/s) for 30 s, and then ramped down to 0.1 1/s. For shear recovery measurements, a constant shear rate of $\dot{\gamma}$ = 0.1 1/s was applied for 100 s, followed by a high shear rate of $\dot{\gamma}$ = 100 1/s for 30 s, and then a low shear rate $\dot{\gamma}$ = 0.1 1/s for another 100 s. An oscillation amplitude sweep was performed at frequencies 1 and 10 Hz over a stress range of 1 Pa $\leq \tau \leq$ 100 Pa. An oscillation frequency sweep was performed at 10 Pa Hz over a frequency range of 0.01 Hz $\leq f \leq$ 100 Hz.

Photorheology. Photorheological measurements were performed at 25 °C using an Anton PAAR Modular Compact Rheometer (Physica MCR 302) in parallel-plate mode and a quartz bottom plate. A Hamamatsu LC8 lamp with a UV-light source (25 mW/cm^2) was placed under the bottom plate. Experiments were performed in flow mode by setting the gap between the two glass plates to 0.3 mm. A constant shear rate of $\dot{\gamma}$ = 0.1 s^{-1} was imposed and the UV irradiation was started after 60 s to allow for the system to stabilize. The viscosity change was monitored as a function of irradiation time.

Photopolymerization Kinetics. Infrared absorption measurements were performed to evaluate polymerization kinetics of ink 2.4% CNC using an IRAffinity-1S Fourier transform infrared spectrophotometer (Shimadzu Corp., Kyoto, Japan) equipped with a diamond ATR attachment and activated by LabSolutions IR software (Shimadzu Corp., Kyoto, Japan). On irradiating unpolymerized ink and fully photopolymerized ink using a light-emitting diode (LED) (365 or 405 nm 50 W LED, Shenzhen Justar Electronic Technology Co., Ltd., China) for 20 s, spectra were acquired by 20 scans of

https://doi.org/10.1021/acs.langmuir.1c00553
Langmuir XXXX, XXX, XXX−XXX

Fourier transform infrared (FTIR) collected over the spectral range of 1800−800 cm^{-1} with instrument resolution of 2 cm^{-1}.

FTIR kinetic monitoring of the polymerization of AA in a 2.4% CNC sample was performed on ∼200 μL of ink dropped on the ATR diamond during light irradiation, followed by acquiring continuous spectra (1 scan per 3 s, with instrument resolution of 8 cm^{-1}) within two ranges, 1800−1500 and 1100−900 cm^{-1}.

Mechanical Testing. Hydrogel objects for the evaluation of mechanical properties were fabricated in molds by exposing to 395 nm light (32V, 8A, Integration Technology Ltd., Oxon, U.K.) for 15 s. Unconfined mechanical tests of solid cylindrical objects (10 mm height, 20 mm diameter) were performed on fully swollen samples (over 72 h), using an Instron universal testing machine (Model 3345, Instron Corp., Norwood, MA) equipped with a 500 N load cell and operated at 5 mm/min. Five replicate specimens were tested under ambient conditions. Young's modulus was calculated up to 15% strain by linear least-squares regression (Scipy.stats.linregress).

3D Printing. Hydrogels were 3D-printed using a Hyrel3D 30M printer (Hyrel International, Inc., Norcross, GA) equipped with an SDS-10 extruder mounted with a 365 nm LED. A 10 mL disposable syringe with a 16-gauge conical tip (1.29 mm) was used throughout the printing process unless indicated otherwise. G-code files were prepared via 3D Slic3r software (Ver. 1.2.9, slic3r.org). The printing rate was set to 5 mm/s, the layer height was set to 0.8 mm, and light irradiation (365 or 405 nm) was applied for 5 s for each printed layer.

Printability. To quantify the printability of ink 2.4% CNC, different hollow square-sized objects consisting of three printed layers were printed (1.29 mm diameter nozzle, printing speed of 10 mm/s) and photographed. Perimeter and area were then measured using FIJI software (ImageJ, National Institute of Health) and the printability was calculated by

$$\mathrm{Pr} = \frac{L^2}{16A} \tag{1}$$

where L and A are the perimeter and area of the printed square, respectively.[34]

Statistical Analysis. All errors indicate a 95% confidence interval (CI) calculated by

$$\mathrm{CI} = \frac{f(t)\cdot\sigma}{\sqrt{N}} \tag{2}$$

where N is the sample size, $f(t)$ is the value of the Student's t-distribution for a specific probability (0.95) and $N - 1$ degrees of freedom, and σ is the sample standard deviation.

RESULTS AND DISCUSSION

Our printing approach is based on combining the pseudoplastic behavior of the ink with rapid fixation of the printed layer. The CNC, which controls the rheological properties of the tested ink, enables obtaining a yield stress value that is sufficient for temporary fixation of a layer printed by extrusion. After each layer is formed, it is exposed to UV light to initiate photopolymerization, which rapidly fixates the permanent shape of the layer. To achieve this, water-based UV-curable inks for DIW, composed of the monomers AA and PEGDA and TPO as the PI, were prepared. As TPO is insoluble in water, we used our developed water-compatible TPO composition, with Brij 58, a nonionic surfactant.[33] Since the viscosity of this photocurable ink is not suitable for DIW printing, we supplemented it with dispersed CNC to tailor the rheological properties.

AA, PEGDA, and CNC were chosen as they have already been reported as biocompatible materials.[35−43] Moreover, the TPO PI was shown to not have any cytotoxic effect on human epithelial colorectal adenocarcinoma cells.[33] However, to minimize the possible negative PI effects, a minimal concentration of TPO was used that enabled rapid curing under a short irradiation time.

Five concentrations of CNC nanoparticles were prepared while maintaining the same concentration of solids in the ink (Table 1). Inks without CNC failed to print objects, as shown as a puddle, in Figure 1A. Additionally, objects printed with the CNC-containing ink, but only exposed to UV irradiation after the objects were printed, failed to maintain their weight and shape beyond a very small number of layers, as seen in the structure slumping (Figure 1B). The combination of CNC and UV curing during printing enabled the printing of objects with multiple highly stable layers (Figure 1C).

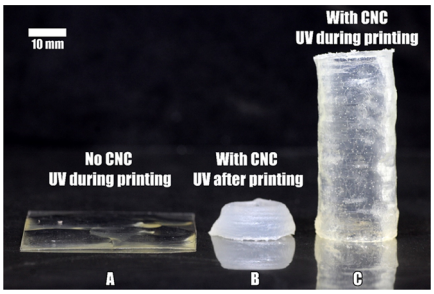

Figure 1. DIW-printed 20 mm diameter tube objects. (A) Tube object failed to be printed with 0% CNC and UV-cured during printing. (B) Tube object failed to be printed with 2.4% CNC and UV-cured after printing; the object is composed of 14 printed layers. (C) Tube object successfully printed with 2.4% CNC and UV-cured during printing. The object contains 32 printed layers.

Rheology. Rheology measurements were performed to examine ink behavior during the different steps of the printing process. First, flow curve experiments were performed to determine how viscosity varies with shear rates. Sufficiently high viscosity at a low shear rate is crucial to avoid ink drippage from the syringe during nonprinting steps, whereas when stress is applied by the syringe piston, viscosity must decrease rapidly to enable extrusion. As shown in Figure 2, shear-thinning occurred only in samples that contained CNC. In addition, the viscosity increased as CNC concentrations increased, while shear-thinning behavior was preserved.

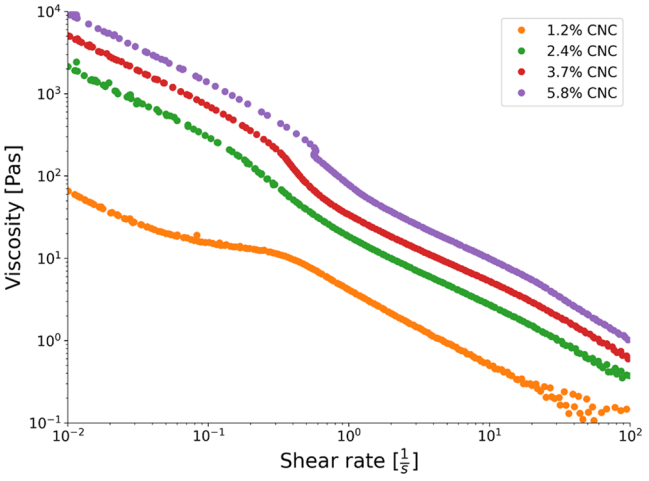

Figure 2. Viscosity as a function of shear rate for different CNC wt % hydrogel inks before exposure to UV light plotted on a double logarithmic scale.

https://doi.org/10.1021/acs.langmuir.1c00553
Langmuir XXXX, XXX, XXX−XXX

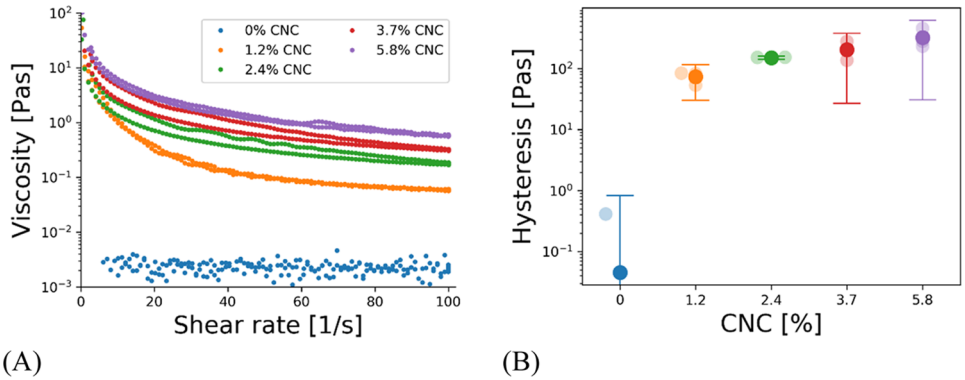

Figure 3. Thixotropy measurement: (A) thixotropy viscosity hysteresis loop and (B) thixotropy index. Light-shaded markers represent actual measurement, dark-shaded markers represent averages, and error bars indicate 95% CI.

In addition to shear-thinning properties, inks used in extrusion-based 3D printers must be thixotropic, which enables them to return to their more viscous state, both in the syringe while not printing and in the printed object, after being extruded. Thixotropy was evaluated by measuring viscosity at three stages: (1) when ramping up the shear rate from $\dot{\gamma}$ = 0.1 1/s to $\dot{\gamma}$ = 100 1/s, which causes a breakdown of the ink structure, seen by the decrease in viscosity, (2) when holding a maximum shear rate for 30 s, and (3) when ramping down the shear rate to $\dot{\gamma}$ = 0.1 1/s while the viscosity recovers by reforming the initial network within the ink. Figure 3A presents the thixotropy behavior of CNC-containing inks. The thixotropy index, calculated from the area of the hysteresis loop from structure breakdown to recovery, represents the energy consumption of this process (Figure 3B). All inks containing CNC exhibited thixotropic behavior.

Shear recovery experiments were performed to evaluate the rheology time dependence of the inks after extrusion. To correlate these measurements with the actual printing shear rate, the maximum shear rate (MSR) was evaluated. MSR of the printer setup was found to be between 75 1/s and 300 1/s, depending on the calculation, which takes into account the rheology dependence on CNC concentration (see Supporting Information Section S1).

In this experiment (Figure 4), a constant low shear rate ($\dot{\gamma}$ = 0.1 1/s, T = 20 °C) was applied for 100 s, followed by a constant high shear rate ($\dot{\gamma}$ = 100 1/s, T = 20 °C) for 30 s, simulating the shear rates, which are applied from the syringe piston. Then, the shear rate was decreased again ($\dot{\gamma}$ = 0.1 1/s, T = 20 °C) and the recovery of the viscosity was measured and compared to the initial viscosity. For all inks tested, a mean of 5 s was required to recover 50% of the viscosity, after applying a shear rate of 100 1/s. Moreover, it was noted that the higher the CNC concentration, the longer it took to reach a steady viscosity. The highest recovery (70.36%) was obtained with the ink containing 2.4% CNC and was reached within 15 s.

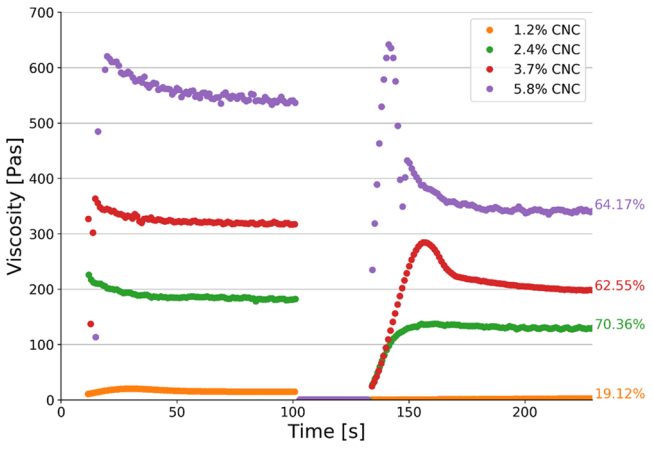

Figure 4. Shear recovery measurements at 100 1/s shear rate. % recovery achieved is indicated to the right of each curve.

Mechanical Properties of Objects in Molds. The mechanical properties of hydrogel objects fabricated in molds from inks containing various CNC concentrations were evaluated by unconfined compression tests (Figure 5A). As shown in Figure 5B, Young's modulus increased with increasing CNC concentrations, with the best precision obtained for the 2.4% ink (raw data is presented in Figure S3). The same trend was observed for the stress-at-break evaluations, which increased three-fold for ink ranging from 0 to 2.4% CNC wt %, without impacting precision (Figure 5D). At higher CNC concentrations, the stress at break continued to increase, but the precision began to decrease. Interestingly, the CNC concentration did not affect strain to break (Figure 5C). It should be noted that the samples prepared with CNC concentrations of 3.7 and 5.8% were brittle, and during the measurements, we observed some cracks, as shown in Figure 5A, which led to a high dispersity of the results. This is also observed in the dispersed results of stress-to-break values (Figure 5D). The loss of precision is assumed to be related to the poor mechanical properties originating from crossing the optimum CNC threshold concentration. This observed behavior of increasing mechanical property till the optimum concentration of CNCs is well observed and can be seen in hydrogels,[44] membranes,[45] and fibers[46] composed of CNC. Based on these results, we concluded that the optimal concentration, in view of both the Young's modulus value and repeatability of measurements, is 2.4%, and subsequent studies were performed at this concentration.

Photorheology. Beyond yield stress, hydrogel inks change their structure from a "solidlike" to a "liquidlike" state (Figures S4 and S5). While printing, the weight of the upper layers exerts stress, which can cause the printed object to collapse, thereby limiting the height of the printed objects. For example, the ink with 2.4% CNC deforms at 50 Pa and, therefore, the maximal achievable height would be 0.5 cm, assuming ρ = 1000 kg/m^3.[12] In practice, the height is even lower due to the impact of capillary forces. To overcome the height

https://doi.org/10.1021/acs.langmuir.1c00553
Langmuir XXXX, XXX, XXX−XXX

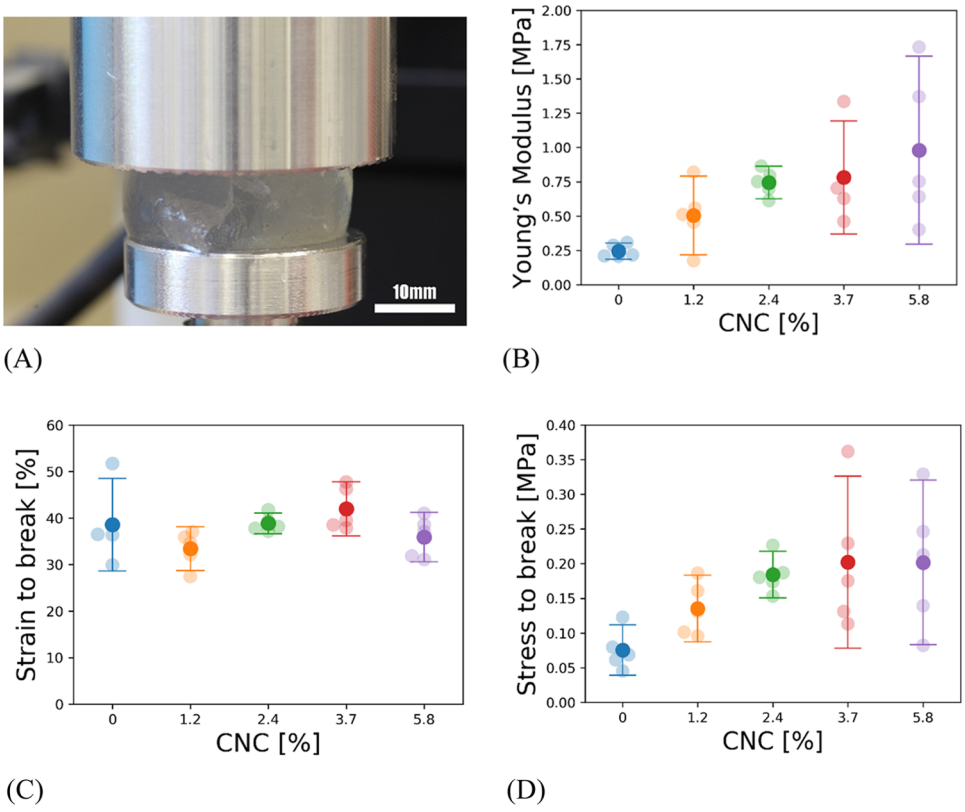

Figure 5. Unconfined compression test of hydrogels integrating various concentrations of CNC. (A) Image of the hydrogel during the test. (B) Young's modulus. (C) Strain to break. (D) Stress to break. Light-shaded markers represent actual measurements, dark-shaded markers represent averages, and error bars indicate 95% CI.

limitation, it is necessary to polymerize the hydrogel before the printing process reaches its yield-stress-dictated height limitation. Photorheology experiments provide a good tool to detect the transition from a liquidlike to a solidlike state via photopolymerization. Therefore, UV photopolymerization was induced to rapidly introduce covalent and permanent cross-links in the hydrogel, which increases the ink rheology temporary fixation yield stress and can withstand the addition of more printed layers.

As described above, based on the observed rheological and mechanical properties, the ink containing 2.4% CNC was selected for photorheological assessment. Photorheology measurements showed that this ink achieves sufficient viscosity that enabled structure fixation within several seconds and required approximately 20 s of irradiation to obtain a fully polymerized hydrogel (Figure 6). It should be noted that the same final viscosity was observed for the CNC-free ink; its initial viscosity was too low for printing by DIW. The same kinetics trend was found by FTIR measurements in which the conversion was evaluated by the disappearance of the C═C stretching mode of AA during irradiation. The details of the kinetics measurements are presented in the Supporting Information Section S2. As shown in Figure S8, after irradiation for 20 s, the conversion was ∼90 and ∼70% for the 405 and 365 nm light, respectively.

3D Printing. To demonstrate the importance of rapid UV curing, 2.4% CNC ink was UV-irradiated during printing or after the entire object was printed (Figures S9 and S10). Figure 7A shows printed tubes (20 mm diameter) subjected to UV irradiation (5 s) after each layer was printed. A gradual increase in height with good fixation of the tube was achieved, with no

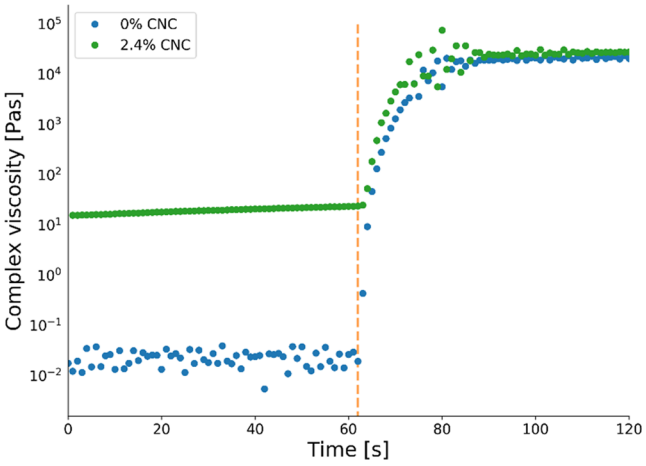

Figure 6. Photorheology characterization of water-soluble PI photopolymerization kinetics for 0 and 2.4% CNC inks. The vertical dashed line indicates the time point at which the light was turned on.

seeming limitation to the final object height. In contrast, when UV irradiation was only applied after the entire tube was printed, the lower part (from layer #4 and onward) of the tube expanded, indicating the collapse of the object (Figure 7B). When reaching layer #14, the supposed-to-be tube object slumped and the printing had to be terminated.

The tubes presented in Figure 7 were printed with a 1.29 mm nozzle diameter to achieve large heights in a short time. The same inks can be printed using much smaller nozzle diameters, which provide enhanced resolution. Figure S11

https://doi.org/10.1021/acs.langmuir.1c00553
Langmuir XXXX, XXX, XXX−XXX

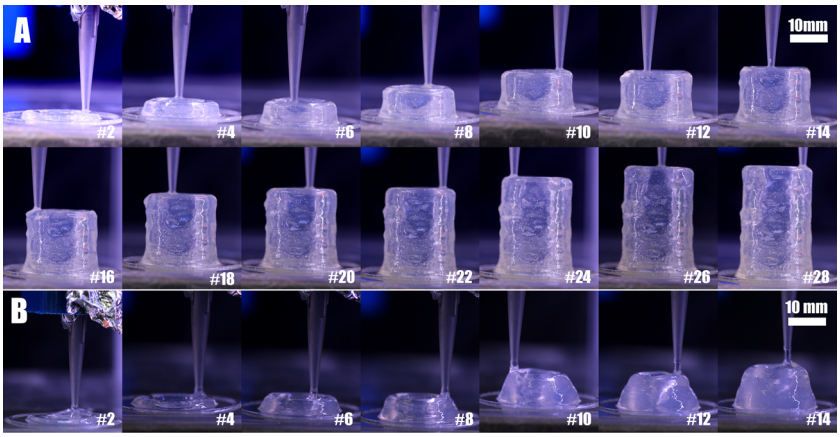

Figure 7. 2.4% CNC DIW-printed 20 mm diameter tube objects photographed at two-layer intervals during the printing process, with rapid UV curing performed (A) after deposition of each layer or (B) after the entire object was printed. The printed layers are indicated at the bottom of each image.

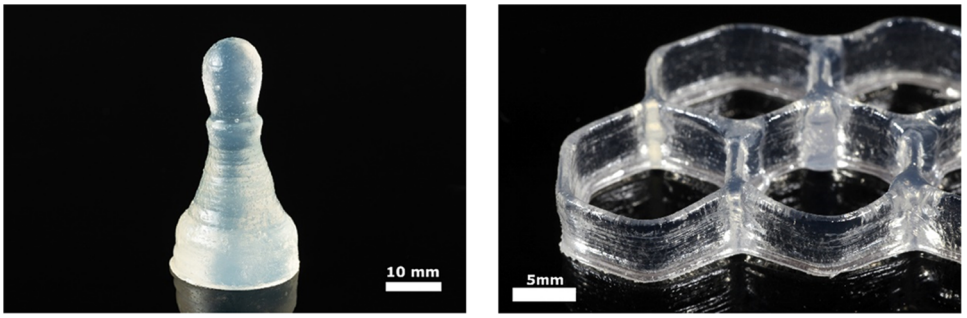

Figure 8. DIW hydrogel structures printed with rapid photopolymerization. (A) Chess pawn cured with 365 nm light. (B) Honeycomb-shaped object cured with 405 nm irradiation.

shows a series of lines printed using the same ink but through a series of nozzles of decreasing diameters.

The printability index describes semiquantitative evaluation based on the circularity of the printed square and shape fidelity of the ink. In this case, high geometric accuracy in the $x-y$ plane results in a printability index of Pr = 1, while Pr < 1 corresponds to a rounded corner square and Pr > 1 corresponds to irregularly shaped transversal geometry. The printability of ink 2.4% CNC was found to be Pr = 0.93, which is very close to value 1, and as would be estimated, for direct ink writing technology, pathway corners are rounded resulting in Pr < 1 (Figure S12). As can be expected, smaller objects have lower printability values, which are governed by nozzle diameter. Moreover, it was found that there is an excellent correlation between the designed area (STL file square area) and the actual measured area, which indicates a reliable and accurate 3D printing system (Figure S13).

To further evaluate the full potential of the ink, a solid cylinder with an 8.3 mm diameter was printed till the extruder volume limitation was reached (up to a pillar height of ∼11 cm), resulting in an aspect ratio of ∼13 (Figure S14). The overhanging ability was evaluated by measurements of upside-down printed cones varying by different angles. The maximum printed angle for 2.4% CNC ink was found to be 30∧0, from which the printed object exhibits rippling (Figure S15).

These experiments were performed using 365 nm UV light, which can display high printing capabilities (Figure 8A) but might be problematic for biomedical applications, due to the negative effect of short-wavelength radiation on cell viability. Figure 8B shows that identical results can be obtained using visible light (405 nm). To test the curing effects of visible light, these same printing experiments were repeated with 405 nm irradiation. As shown in Figure S16, the same degree of fixation was achieved, without compromising the printing speed or resolution.

CONCLUSIONS

Acrylic acid-based hydrogels reinforced with CNC were 3D-printed and photopolymerized using a water-compatible PI. The CNC imparted a unique rheological behavior, which was expressed by orders of magnitude different behaviors at low versus high shear rates and fast and high shear recovery, without compromising ink printability. Rapid photopolymerization performed immediately after printing each layer overcame the common height limit of DIW printing of hydrogels and enabled the fabrication of objects with a high aspect ratio. The presented approach enabled the shortest irradiation time under extremely low concentrations of PI, including possible curing by 405 nm light, which is important for maintaining viability in bioinks.

ASSOCIATED CONTENT

Supporting Information

The Supporting Information is available free of charge at https://pubs.acs.org/doi/10.1021/acs.langmuir.1c00553.

https://doi.org/10.1021/acs.langmuir.1c00553
Langmuir XXXX, XXX, XXX−XXX

Summary of photocurable hydrogels based on one-time illumination and based on build time; estimating printing maximum shear rate of the ink; raw data of the unconfined compression test; oscillation amplitude sweep and frequency sweep; polymerization kinetics of acrylic acid using a FTIR spectrophotometer; photos of printed tubes with and without rapid photopolymerization; 3D geometrical capabilities; and comparison between different wavelength irradiations (PDF)

AUTHOR INFORMATION

Corresponding Authors

Oded Shoseyov − *Plant Sciences and Genetics in Agriculture, The Hebrew University of Jerusalem, Rehovot 7610001, Israel*; Email: shoseyov@agri.huji.ac.il

Shlomo Magdassi − *Institute of Chemistry, The Hebrew University of Jerusalem, Jerusalem 9190401, Israel*; orcid.org/0000-0002-6794-0553; Email: magdassi@mail.huji.ac.il

Authors

Doron Kam − *Institute of Chemistry, The Hebrew University of Jerusalem, Jerusalem 9190401, Israel; Plant Sciences and Genetics in Agriculture, The Hebrew University of Jerusalem, Rehovot 7610001, Israel*; orcid.org/0000-0002-5119-965X

Ariel Braner − *Institute of Chemistry, The Hebrew University of Jerusalem, Jerusalem 9190401, Israel; Alpha Program, Future Scientist Center, Jerusalem 9190401, Israel*

Avi Abouzglo − *Institute of Chemistry, The Hebrew University of Jerusalem, Jerusalem 9190401, Israel*

Liraz Larush − *Institute of Chemistry, The Hebrew University of Jerusalem, Jerusalem 9190401, Israel*

Annalisa Chiappone − *Department of Applied Science and Technology, Politecnico di Torino, Torino 10129, Italy*; orcid.org/0000-0003-4651-1140

Complete contact information is available at: https://pubs.acs.org/10.1021/acs.langmuir.1c00553

Author Contributions

The manuscript was written through the contributions of all authors. All authors have given approval to the final version of the manuscript.

Funding

We thank the Ministry of Science Technology and Space, Israel, for financial support (3-15638).

Notes

The authors declare no competing financial interest.

ACKNOWLEDGMENTS

The authors would like to thank Prof. Morton M. Denn for fruitful discussions on rheology. They also greatly thank Sartomer-Arkema for providing the PEGDA sample.

ABBREVIATIONS

DIW, direct ink writing; CNC, cellulose nanocrystals; PI, photoinitiator; PDMA, poly(*N*,*N*-dimethacrylamide); LAP, lithium phenyl-2,4,6-trimethylbenzoylphosphinate; AA, acrylic acid; IPA, isopropanol; TPO, 2,4,6-trimethylbenzoyl-diphenyl-phosphine oxide; CI, confidence interval; PEGDA, poly(ethylene glycol) diacrylate

REFERENCES

(1) Martin, J. H.; Yahata, B. D.; Hundley, J. M.; Mayer, J. A.; Schaedler, T. A.; Pollock, T. M. 3D Printing of High-Strength Aluminium Alloys. *Nature* **2017**, *549*, 365−369.

(2) Tepylo, N.; Huang, X.; Patnaik, P. C. Laser-Based Additive Manufacturing Technologies for Aerospace Applications. *Adv. Eng. Mater.* **2019**, *21*, No. 1900617.

(3) Dawood, A.; Marti, B. M.; Sauret-Jackson, V.; Darwood, A. 3D Printing in Dentistry. *Br. Dent. J.* **2015**, *219*, 521−529.

(4) Sachyani Keneth, E.; Kamyshny, A.; Totaro, M.; Beccai, L.; Magdassi, S. 3D Printing Materials for Soft Robotics. *Adv. Mater.* **2021**, *33*, No. 2003387.

(5) Mathew, E.; Pitzanti, G.; Larrañeta, E.; Lamprou, D. A. Three-Dimensional Printing of Pharmaceuticals and Drug Delivery Devices. *Pharmaceutics* **2020**, *12*, No. 266.

(6) Noor, N.; Shapira, A.; Edri, R.; Gal, I.; Wertheim, L.; Dvir, T. 3D Printing of Personalized Thick and Perfusable Cardiac Patches and Hearts. *Adv. Sci.* **2019**, *6*, No. 1900344.

(7) Jammalamadaka, U.; Tappa, K. Recent Advances in Biomaterials for 3D Printing and Tissue Engineering. *J. Funct. Biomater.* **2018**, *9*, No. 22.

(8) Dong, Y.; Wang, S.; Ke, Y.; Ding, L.; Zeng, X.; Magdassi, S.; Long, Y. 4D Printed Hydrogels: Fabrication, Materials, and Applications. *Adv. Mater. Technol.* **2020**, *5*, No. 2000034.

(9) Ge, Q.; Chen, Z.; Cheng, J.; Zhang, B.; Zhang, Y. F.; Li, H.; He, X.; Yuan, C.; Liu, J.; Magdassi, S.; Qu, S. 3D Printing of Highly Stretchable Hydrogel with Diverse UV Curable Polymers. *Sci. Adv.* **2021**, *7*, No. eaba4261.

(10) Cui, X.; Breitenkamp, K.; Finn, M. G.; Lotz, M.; D'Lima, D. D. Direct Human Cartilage Repair Using Three-Dimensional Bioprinting Technology. *Tissue Eng., Part A* **2012**, *18*, 1304−1312.

(11) Fonseca, A. C.; Melchels, F. P. W.; Ferreira, M. J. S.; Moxon, S. R.; Potjewyd, G.; Dargaville, T. R.; Kimber, S. J.; Domingos, M. Emulating Human Tissues and Organs: A Bioprinting Perspective Toward Personalized Medicine. *Chem. Rev.* **2020**, *120*, 11128−11174.

(12) M'Barki, A.; Bocquet, L.; Stevenson, A. Linking Rheology and Printability for Dense and Strong Ceramics by Direct Ink Writing. *Sci. Rep.* **2017**, *7*, No. 6017.

(13) Napadensky, E. Inkjet 3D Printing. In *The Chemistry of Inkjet Inks*; Magdassi, S., Eds.; 2009; pp 255−268.

(14) Mora-Boza, A.; Włodarczyk-Biegun, M. K.; Del Campo, A.; Vázquez-Lasa, B.; Román, J. S. Glycerylphytate as an Ionic Crosslinker for 3D Printing of Multi-Layered Scaffolds with Improved Shape Fidelity and Biological Features. *Biomater. Sci.* **2020**, *8*, 506−516.

(15) Zhuang, P.; Ng, W. L.; An, J.; Chua, C. K.; Tan, L. P. Layer-by-Layer Ultraviolet Assisted Extrusion-Based (UAE) Bioprinting of Hydrogel Constructs with High Aspect Ratio for Soft Tissue Engineering Applications. *PLoS One* **2019**, *14*, No. e0216776.

(16) Pawar, A. A.; Saada, G.; Cooperstein, I.; Larush, L.; Jackman, J. A.; Tabaei, S. R.; Cho, N.-J. J.; Magdassi, S. High-Performance 3D Printing of Hydrogels by Water-Dispersible Photoinitiator Nanoparticles. *Sci. Adv.* **2016**, *2*, No. e1501381.

(17) Pawar, A. A.; Saada, G.; Cooperstein, I.; Larush, L.; Jackman, J. A.; Tabaei, S. R.; Cho, N.-J. J.; Magdassi, S. High-Performance 3D Printing of Hydrogels by Water-Dispersible Photoinitiator Nanoparticles. *Sci. Adv.* **2016**, *2*, No. ee1501381.

(18) Kam, D.; Layani, M.; BarkaiMinerbi, S.; Orbaum, D.; Abrahami BenHarush, S.; Shoseyov, O.; Magdassi, S. Additive Manufacturing of 3D Structures Composed of Wood Materials. *Adv. Mater. Technol.* **2019**, *4*, No. 1900158.

(19) Kam, D.; Chasnitsky, M.; Nowogrodski, C.; Braslavsky, I.; Abitbol, T.; Magdassi, S.; Shoseyov, O. Direct Cryo Writing of Aerogels Via 3D Printing of Aligned Cellulose Nanocrystals Inspired by the Plant Cell Wall. *Colloids Interfaces* **2019**, *3*, No. 46.

(20) Beck-Candanedo, S.; Roman, M.; Gray, D. G. Effect of Reaction Conditions on the Properties and Behavior of Wood Cellulose Nanocrystal Suspensions. *Biomacromolecules* **2005**, *6*, 1048−1054.

(21) Abitbol, T.; Kam, D.; Levi-Kalisman, Y.; Gray, D. G.; Shoseyov, O. Surface Charge Influence on the Phase Separation and Viscosity of Cellulose Nanocrystals. *Langmuir* **2018**, *34*, 3925−3933.
(22) De France, K. J.; Hoare, T.; Cranston, E. D. Review of Hydrogels and Aerogels Containing Nanocellulose. *Chem. Mater.* **2017**, *29*, 4609−4631.
(23) Wang, J.; Siqueira, G.; Müller, G.; Rentsch, D.; Huch, A.; Tingaut, P.; Levalois-Grützmacher, J.; Grützmacher, H. Synthesis of New Bis(Acyl)Phosphane Oxide Photoinitiators for the Surface Functionalization of Cellulose Nanocrystals. *Chem. Commun.* **2016**, *52*, 2823−2826.
(24) Siqueira, G.; Kokkinis, D.; Libanori, R.; Hausmann, M. K.; Gladman, A. S.; Neels, A.; Tingaut, P.; Zimmermann, T.; Lewis, J. A.; Studart, A. R. Cellulose Nanocrystal Inks for 3D Printing of Textured Cellular Architectures. *Adv. Funct. Mater.* **2017**, *27*, No. 1604619.
(25) Yang, J.; Han, C. R.; Xu, F.; Sun, R. C. Simple Approach to Reinforce Hydrogels with Cellulose Nanocrystals. *Nanoscale* **2014**, *6*, 5934−5943.
(26) Kelly, J. A.; Shukaliak, A. M.; Cheung, C. C. Y.; Shopsowitz, K. E.; Hamad, W. Y.; MacLachlan, M. J. Responsive Photonic Hydrogels Based on Nanocrystalline Cellulose. *Angew. Chem., Int. Ed.* **2013**, *52*, 8912−8916.
(27) Wang, P.-X.; Hamad, W. Y.; MacLachlan, M. J. Structure and Transformation of Tactoids in Cellulose Nanocrystal Suspensions. *Nat. Commun.* **2016**, *7*, No. 11515.
(28) Zhang, Z.; Liu, R.; Zepeda, H.; Zeng, L.; Qiu, J.; Wang, S. 3D Printing Super Strong Hydrogel for Artificial Meniscus. *ACS Appl. Polym. Mater.* **2019**, *1*, 2023−2032.
(29) Frost, B.; Sutliff, B. P.; Thayer, P.; Bortner, M. J.; Foster, E. J. Gradient Poly(Ethylene Glycol) Diacrylate and Cellulose Nanocrystals Tissue Engineering Composite Scaffolds via Extrusion Bioprinting. *Front. Bioeng. Biotechnol.* **2019**, *7*, No. 280.
(30) Li, V. C. F.; Kuang, X.; Mulyadi, A.; Hamel, C. M.; Deng, Y.; Qi, H. J. 3D Printed Cellulose Nanocrystal Composites through Digital Light Processing. *Cellulose* **2019**, *26*, 3973−3985.
(31) Palaganas, N. B.; Mangadlao, J. D.; De Leon, A. C. C.; Palaganas, J. O.; Pangilinan, K. D.; Lee, Y. J.; Advincula, R. C. 3D Printing of Photocurable Cellulose Nanocrystal Composite for Fabrication of Complex Architectures via Stereolithography. *ACS Appl. Mater. Interfaces* **2017**, *9*, 34314−34324.
(32) Wang, J.; Chiappone, A.; Roppolo, I.; Shao, F.; Fantino, E.; Lorusso, M.; Rentsch, D.; Dietliker, K.; Pirri, C. F.; Grützmacher, H. All-in-One Cellulose Nanocrystals for 3D Printing of Nanocomposite Hydrogels. *Angew. Chem., Int. Ed.* **2018**, *57*, 2353−2356.
(33) Larush, L.; Kaner, I.; Fluksman, A.; Tamsut, A.; Pawar, A. A.; Lesnovski, P.; Benny, O.; Magdassi, S. 3D Printing of Responsive Hydrogels for Drug-Delivery Systems. *J. 3D Print. Med.* **2017**, *1*, 219−229.
(34) Liliang, O.; Rui, Y.; Yu, Z.; Wei, S. Effect of Bioink Properties on Printability and Cell Viability for 3D Bioplotting of Embryonic Stem Cells. *Biofabrication* **2016**, *8*, No. 35020.
(35) Patel, D. K.; Dutta, S. D.; Shin, W. C.; Ganguly, K.; Lim, K. T. Fabrication and Characterization of 3D Printable Nanocellulose-Based Hydrogels for Tissue Engineering. *RSC Adv.* **2021**, *11*, 7466−7478.
(36) ALGhanem, A.; Fernandes, G.; Visser, M.; Dziak, R.; Renné, W. G.; Sabatini, C. Biocompatibility and Bond Degradation of Poly-Acrylic Acid Coated Copper Iodide-Adhesives. *Dent. Mater.* **2017**, *33*, e336−e347.
(37) Luo Zheng, L.; Vanchinathan, V.; Dalal, R.; Noolandi, J.; Waters, D. J.; Hartmann, L.; Cochran, J. R.; Frank, C. W.; Yu, C. Q.; Ta, C. N. Biocompatibility of Poly(Ethylene Glycol) and Poly(Acrylic Acid) Interpenetrating Network Hydrogel by Intrastromal Implantation in Rabbit Cornea. *J. Biomed. Mater. Res., Part A* **2015**, *103*, 3157−3165.
(38) Wittemann, A.; Azzam, T.; Eisenberg, A. Biocompatible Polymer Vesicles from Biamphiphilic Triblock Copolymers and Their Interaction with Bovine Serum Albumin. *Langmuir* **2007**, *23*, 2224−2230.
(39) Deng, X.; Huang, B.; Hu, R.; Chen, L.; Tang, Y.; Lu, C.; Chen, Z.; Zhang, W.; Zhang, X. 3D Printing of Robust and Biocompatible Poly(Ethylene Glycol)Diacrylate/Nano-Hydroxyapatite Composites-viacontinuous Liquid Interface Production. *J. Mater. Chem. B* **2021**, *9*, 1315−1324.
(40) Słota, D.; Florkiewicz, W.; Sobczak-Kupiec, A. Ceramic-Polymer Coatings on Ti-6Al-4V Alloy Modified with L-Cysteine in Biomedical Applications. *Mater. Today Commun.* **2020**, *25*, No. 101301.
(41) Deng, Z.; Qian, T.; Hang, F. Three-Dimensional Printed Hydrogels with High Elasticity, High Toughness, and Ionic Conductivity for Multifunctional Applications. *ACS Biomater. Sci. Eng.* **2020**, *6*, 7061−7070.
(42) Nguyen, V. T. A.; De Pauw-Gillet, M. C.; Sandre, O.; Gauthier, M. Biocompatible Polyion Complex Micelles Synthesized from Arborescent Polymers. *Langmuir* **2016**, *32*, 13482−13492.
(43) Liang, J.; Struckhoff, J. J.; Hamilton, P. D.; Ravi, N. Preparation and Characterization of Biomimetic β-Lens Crystallins Using Single-Chain Polymeric Nanoparticles. *Langmuir* **2017**, *33*, 7660−7668.
(44) Gonzalez, J. S.; Ludueña, L. N.; Ponce, A.; Alvarez, V. A. Poly(Vinyl Alcohol)/Cellulose Nanowhiskers Nanocomposite Hydrogels for Potential Wound Dressings. *Mater. Sci. Eng., C* **2014**, *34*, 54−61.
(45) Kim, S.; Xiong, R.; Tsukruk, V. V. Probing Flexural Properties of Cellulose Nanocrystal−Graphene Nanomembranes with Force Spectroscopy and Bulging Test. *Langmuir* **2016**, *32*, 5383−5393.
(46) Ureña-Benavides, E. E.; Brown, P. J.; Kitchens, C. L. Effect of Jet Stretch and Particle Load on Cellulose Nanocrystal−Alginate Nanocomposite Fibers. *Langmuir* **2010**, *26*, 14263−14270.

https://doi.org/10.1021/acs.langmuir.1c00553
Langmuir XXXX, XXX, XXX−XXX